LQG Based Model Predictive Control for Gust Load Alleviation

Xiang Liu[a], Qin Sun[a,*] and J. E. Cooper[b]

[a] *School of Aeronautics, Northwestern Polytechnical University, Xi'an, China*
[b] *Department of Aerospace Engineering, University of Bristol, Bristol, UK*

Abstract

A linear quadratic Gaussian (LQG) based model predictive control (MPC) method is proposed to alleviate the dynamic gust loads of flexible aircrafts flying through turbulence, utilizing look-ahead information of the turbulence via light detection and ranging (LIDAR) systems or on board alpha probe. The new method features both infinite prediction horizon and infinite control horizon. The forepart of the infinite control sequence consists of a few online optimized variables, and the rest are outputs of an LQG controller, designed offline using an improved LQG method. The advantages of the proposed method are twofold. Firstly, the stability property of the controlled system is improved due to application of the infinite prediction horizon and the LQG controller. Secondly, adoption of an infinite control horizon not only improves the control performance, but also greatly reduces the number of online optimized control variables whilst retaining control performance. Furthermore, a technique to tackle the effects of control delay is also designed. The effectiveness and advantages of the proposed approach are demonstrated through numerical results using a general transport aircraft model.

Keywords: Gust load alleviation; Model predictive control; Linear quadratic Gaussian method; Control delay

1. Introduction

Active gust load alleviation (GLA) systems, i.e., systems used to reduce the load impact of flexible aircrafts encountering turbulence through deflecting aerodynamic control surfaces, has recently become prevalent for aircraft designers since these systems are beneficial for reducing the weight and increasing the fatigue life of commercial aircraft. Various control techniques have been studied in the past several decades, e.g. linear quadratic Gaussian (LQG) theory [1,2], H_∞ control theory [3,4] and μ synthesis theory [5,6]. As well the aforementioned feedback control methods using the concept of active damping, feedforward control methods are also frequently studied which adopt suitable reference signals for the purpose of active gust load compensation. For example, Hahn and Koenig [7] used a signal from a nose-boom-mounted alpha probe as reference of vertical gust in the design of the feedforward controller, and Dornheim [8] used static pressure measurements as reference of lateral gust in the design of the vertical stabilizer. To achieve both GLA and ride comfort improvement, a robust feedforward approach was proposed by Hecker and Hahn [9] on an airliner with limited uncertainty. A combination of feedforward and feedback approach was also proposed by Alam et al. [10] to increase the robust performance of the GLA system.

To account for the time-varying characteristics of the aircraft dynamics, gain scheduling is extensively studied in recent years by different researchers. To achieve GLA, Zeng et al. [11] designed a single-input single-output adaptive feedforward controller, with variations of aircraft configuration taken into account by a real time system identification algorithm. Afterwards, Wildschek et al. [12]

* Corresponding author. E-mail: sunqin@nwpu.edu.cn.

proposed a multi-input multi-output adaptive feedforward controller with detailed stability property analysis. Using the preview information from an onboard alpha probe, Zhao et al. [13] designed an adaptive feedforward controller, with its long-term numerical stability guaranteed by the circular leaky least mean-squared (CLLMS) algorithm. In the research of Fonte et al. [14], a static output feedback controller is designed within quadratic optimal framework for GLA. The simple structure of the static output feedback controller facilitates application of scheduled solution.

Based on the advantages of new modeling method, intelligent materials and morphing wings, some other methods have been proposed for aircraft control. For example, using data-based model, Lew and Juang [15] presented a robust generalized predictive control method, which was successfully applied for active flutter suppression of a benchmark wind tunnel model. The uncertainty directly quantified from measured data is used in control design. Based on the work of Lew and Juang [15], Dai et al. [16] developed gust response alleviation system with the gust input approximated by polynomials of flow velocities. Comparison between the simulated closed-loop response and experimental results indicates that the wing tip acceleration response is greatly alleviated. Considering the advantages of piezoelectric materials including low weight, high energy efficiency and flexible distribution, many researchers have designed and tested GLA systems with piezoelectric actuators [17,18]. Moreover, the research of Cooper et al. [19] showed that a chiral morphing wingtip device can be used to improve aerodynamic performance and develop a passive gust load alleviation capability. Afterwards, the use of nonlinear negative stiffness folding wingtips as a gust load alleviation device was investigated by Castrichini et al. [20]. It is found that significant reductions in the dynamic loads are possible.

Recently, model predictive control (MPC) technique has been identified to be advantageous for the design of GLA systems due to explicit consideration of inputs and states constraints. Furthermore, look-ahead information about the gust encounters can be readily utilized in the MPC design. Haghighat et al. [21] developed a GLA system for a very flexible aircraft based on an MPC method with prediction enhancement, and Wang et al. [22] proposed a nonlinear MPC method to reduce the gust loads of flexible aircraft modeled by geometrically-nonlinear beams. However, these methods are based on the assumption of perfect state availability. For practical applications, Kalman filters are often used to obtain estimates of the state information through available measurements [23,24]. In the work of Giesseler et al. [23], light detection and ranging (LIDAR) systems are used to provide look-ahead measurements of incoming gust. To ensure the nominal stability of the MPC applied for GLA, Kopf et al. [24] presented a sufficient condition based on a stabilizing terminal penalty.

The MPC technique has also been extensity studied for control design of aircraft if only rigid dynamics are considered [25-27], while research of its application on GLA systems is relatively limited, mainly because of the large model orders introduced by structural flexibility and the lack of research on the relevant stability aspects. Besides, since structural nonlinearities, variations of flight parameters and modeling errors all contribute to uncertainties of the plant model, the robust stability of the MPC controller should be emphasized around the designing point. Furthermore, the effect of control delay should also be considered since MPC requires an optimization problem to be solved online at each sampling time and delays are likely to have a major effect.

In this paper, a new MPC technique is developed combining the traditional MPC technique [28] and a recently proposed LQG technique [29], which is an improvement of the classical LQG method with better robust performance and robust stability. Look-ahead information of the turbulence is also utilized via LIDAR systems or on board alpha probe. The novelty of this framework lies in the realization of both infinite prediction and infinite control horizon in the MPC algorithm. The infinite control signal sequence is divided into two parts. The forepart consists of a small number of online optimized variables, and the second part is output of the offline designed LQG controller. The

advantages of the proposed method are as follows. Firstly, not only is the nominal stability of the controlled system guaranteed due to application of infinite prediction horizon, but the robust stability of the MPC controller is improved due to the specially designed LQG controller. Secondly, adoption of infinite control horizon not only improves the control performance, but is also beneficial for effectively reducing the number of online optimized control variables whilst retaining control performance, and thus reducing the computation burden. Furthermore, technique to tackle the effects of any control delay is also designed.

Section 2 of this paper briefly presents the aeroelastic model of a flexible aircraft. Section 3 describes in detail the newly proposed LQG based MPC method for GLA. Afterward, numerical examples are given in Section 4 and conclusions are made in Section 5.

2. Aeroelastic Model

To simulate the response of a flexible aircraft during gust encounters, a fully multi-disciplinary model is usually adopted. Different aspects that should be included are: flight mechanics, aeroelastic effects, actuator dynamics, control systems and dynamic gust loads. Since the large rigid-body motions, nonlinear unsteady dynamics and sometimes nonlinear structural deformations all result in model complexity and nonlinearity, a time-domain linearized reduced model needs to be built to facilitate control design. Various methods to construct the integrated model and techniques to derive the reduce model have been proposed [21,22,30].

For simplicity, this paper constructs a linear reduced model directly as in [31]. The structural model is built using modal approach and the unsteady aerodynamic model is built with the panel method. Note that both rigid-body and elastic modes are considered. Discretization of the resultant state space model is

$$\begin{aligned} \boldsymbol{x}(k+1) &= \mathbf{A}\boldsymbol{x}(k) + \mathbf{B}\boldsymbol{u}(k) + \mathbf{B}_{\mathrm{g}} w_{\mathrm{g}}(k) \\ \boldsymbol{y}_{\mathrm{s}}(k) &= \mathbf{C}_{\mathrm{s}}\boldsymbol{x}(k) + \mathbf{D}_{\mathrm{s}} w_{\mathrm{g}}(k) \\ \boldsymbol{y}_{\mathrm{c}}(k) &= \mathbf{C}_{\mathrm{c}}\boldsymbol{x}(k) + \mathbf{D}_{\mathrm{c}} w_{\mathrm{g}}(k) \end{aligned} \tag{1}$$

where k is the current sampling time, $\boldsymbol{x}$ is the state vector, $\boldsymbol{u}$ is the control input, w_{g} is the gust velocity, $\boldsymbol{y}_{\mathrm{s}}$ is the sensor output, and $\boldsymbol{y}_{\mathrm{c}}$ is the controlled output. $\mathbf{A}$, $\mathbf{B}$, $\mathbf{B}_{\mathrm{g}}$, $\mathbf{C}_{\mathrm{s}}$, $\mathbf{D}_{\mathrm{s}}$, $\mathbf{C}_{\mathrm{c}}$, and $\mathbf{D}_{\mathrm{c}}$ are the open-loop system matrices. The system in Eq. (1) is required to be controllable through $\boldsymbol{u}$ and observable through $\boldsymbol{y}_{\mathrm{s}}$. The mode displacement method [31] is used to calculate the dynamic loads in $\boldsymbol{y}_{\mathrm{c}}$. Additionally, the gust velocity w_{g} is assumed to be directly measured by LIDAR systems or on board alpha probe. Method to calculate the gust-induced angle of attack from the alpha probe and the inertial measurement can be founded in [12].

3. LQG based MPC Design for GLA

Traditionally, the rigid-body tracking system and the structural control system are designed separately and interaction between these two aspects is avoided by using notch filters. But such an approach will become infeasible for aircraft with high flexibility due to the strong coupling between rigid-body dynamics and structural dynamics. Thus, the design of unified controllers which considers both the rigid-body dynamics and structural flexibility becomes necessary. Furthermore, the low damping of the structure leads to challenges when designing the state observer. These difficulties are addressed in this section through a novel improvement of the traditional MPC method.

3.1 Traditional MPC

MPC is a well-known discrete method in optimal control [32]. In MPC, the control inputs are calculated at each sampling time through solving a constrained optimization problem over a finite

control horizon, specified by the number of future control steps. Because of the large improvement in computer hardware and development of quadratic programming (QP) algorithms, application of MPC technique on systems with fast dynamics is becoming promising [26,33].

The block diagram of output feedback MPC system for GLA is shown in Fig. 1. A Kalman filter is used to estimate the plant states using available information. At each sampling time, the MPC controller calculates the future control inputs through QP algorithm, taking the estimated states and the measured gust velocity as inputs, and then the first element of the optimal solution is applied via the actuators.

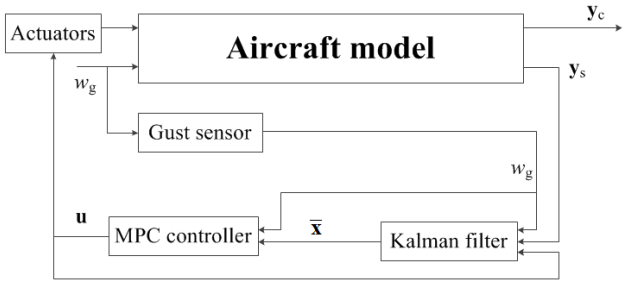

Fig. 1. Block diagram of MPC system for GLA

The future states and outputs of the aircraft model are estimated by the equation

$$\begin{aligned}\bar{\boldsymbol{x}}(k+1|k) &= \bar{\mathbf{A}}\bar{\boldsymbol{x}}(k|k-1)+\bar{\mathbf{B}}\boldsymbol{u}(k)+\bar{\mathbf{B}}_g w_g(k)+\mathbf{K}\left(\boldsymbol{y}_s(k)-\bar{\boldsymbol{y}}_s(k|k-1)\right)\\ \bar{\boldsymbol{y}}_c(k|k-1) &= \bar{\mathbf{C}}_c\bar{\boldsymbol{x}}(k|k-1)+\bar{\mathbf{D}}_c w_g(k)\end{aligned} \tag{2}$$

where the first equation corresponds to the Kalman filter. $\bar{\boldsymbol{x}}(k+1|k)$ is the estimate of the state $\boldsymbol{x}$ at sampling time $k+1$ based on the available information at sampling time k. Similarly, $\bar{\boldsymbol{y}}_c(k|k-1)$ is the estimate of $\boldsymbol{y}_c$ at sampling time k based on the available information at sampling time $k-1$. $\mathbf{K}$ is a feedback gain matrix used to improve the estimation accuracy based on the estimator error $\bar{\boldsymbol{d}}(k|k)$ defined by

$$\bar{\boldsymbol{d}}(k|k)=\boldsymbol{y}_s(k)-\bar{\boldsymbol{y}}_s(k|k-1) \tag{3}$$

The methodology to obtain $\mathbf{K}$ will be discussed briefly in Section 3.2. In principle, $\bar{\mathbf{A}}$, $\bar{\mathbf{B}}$, $\bar{\mathbf{B}}_g$, $\bar{\mathbf{C}}_c$ and $\bar{\mathbf{D}}_c$ in Eq. (2) should be constructed using the same flight parameters and structural parameters as in Eq. (1), but in the test section different values will be chosen to test the robust performance of the designed controller. The model used to construct these matrices is defined as the internal model and the real aircraft model is denoted as the plant model.

The optimal values of the control inputs, $\boldsymbol{u}(k)$, are obtained based on their influence on the future values of $\bar{\boldsymbol{y}}_c$, which are to be minimized. If the future values of $\bar{\boldsymbol{y}}_c$ are to be considered in the following N sampling periods (i.e. the prediction horizon is N), the following assumption can be made regarding the estimator error due to unavailability of future information such that

$$\bar{\boldsymbol{d}}(k+i|k)=0, \quad i=1,\cdots,N \tag{4}$$

Note that different assumptions can be made on $\bar{\boldsymbol{d}}(k+i|k)$ when considering steady-state offset [28], but this is not studied in this paper. If the control horizon is also chosen to be N, the following prediction equations are obtained, based on Eq. (2) and Eq. (4) with

$$\boldsymbol{\psi}(k)=\mathbf{H}\boldsymbol{m}(k)+\mathbf{Y}_x\bar{\boldsymbol{x}}(k|k-1)+\mathbf{Y}_v\boldsymbol{v}(k)+\mathbf{Y}_d\bar{\boldsymbol{d}}(k|k) \tag{5}$$

where $\boldsymbol{\psi}(k)$ is the future estimates of $\bar{\boldsymbol{y}}_c$

$$\boldsymbol{\psi}(k)=\left[\bar{\boldsymbol{y}}_c^{\,T}(k+1|k) \quad \bar{\boldsymbol{y}}_c^{\,T}(k+2|k) \quad \cdots \quad \bar{\boldsymbol{y}}_c^{\,T}(k+N|k)\right]^T \tag{6}$$

$\boldsymbol{m}(k)$ is a vector of future control inputs

$$\boldsymbol{m}(k)=\left[\boldsymbol{u}^T(k|k) \quad \boldsymbol{u}^T(k+1|k) \quad \cdots \quad \boldsymbol{u}^T(k+N-1|k)\right]^T \tag{7}$$

and $\boldsymbol{v}(k)$ is a vector of the measurement values of the future gust velocity

$$\boldsymbol{v}(k)=\begin{bmatrix} w_g(k) & w_g(k+1) & \cdots & w_g(k+N-1) \end{bmatrix} \tag{8}$$

Note that if the lead time of the LIDAR system or the alpha probe cannot cover the scope of $\boldsymbol{v}(k)$ in Eq. (8), the unmeasured part of $\boldsymbol{v}(k)$ should be filled with zeros. The relevant matrices in Eq. (5) are given by

$$\mathbf{H}=\begin{bmatrix} \bar{\boldsymbol{C}}_{\mathrm{c}}\bar{\boldsymbol{B}} & 0 & \cdots & 0 \\ \bar{\boldsymbol{C}}_{\mathrm{c}}\bar{\mathbf{A}}\bar{\boldsymbol{B}} & \bar{\boldsymbol{C}}_{\mathrm{c}}\bar{\boldsymbol{B}} & \cdots & 0 \\ \cdots & \cdots & \cdots & \cdots \\ \bar{\boldsymbol{C}}_{\mathrm{c}}\bar{\mathbf{A}}^{N-1}\bar{\boldsymbol{B}} & \bar{\boldsymbol{C}}_{\mathrm{c}}\bar{\mathbf{A}}^{N-2}\bar{\boldsymbol{B}} & \cdots & \bar{\boldsymbol{C}}_{\mathrm{c}}\bar{\boldsymbol{B}} \end{bmatrix} \tag{9}$$

$$\mathbf{Y}_{\boldsymbol{x}}=\begin{bmatrix} \left(\bar{\boldsymbol{C}}_{\mathrm{c}}\bar{\mathbf{A}}\right)^T & \left(\bar{\boldsymbol{C}}_{\mathrm{c}}\bar{\mathbf{A}}^2\right)^T & \cdots & \left(\bar{\boldsymbol{C}}_{\mathrm{c}}\bar{\mathbf{A}}^N\right)^T \end{bmatrix}^T \tag{10}$$

$$\mathbf{Y}_{\boldsymbol{v}}=\begin{bmatrix} \bar{\boldsymbol{C}}_{\mathrm{c}}\bar{\boldsymbol{B}}_{\mathrm{g}} & \bar{\boldsymbol{D}}_{\mathrm{c}} & 0 & \cdots & 0 \\ \bar{\boldsymbol{C}}_{\mathrm{c}}\bar{\mathbf{A}}\bar{\boldsymbol{B}}_{\mathrm{g}} & \bar{\boldsymbol{C}}_{\mathrm{c}}\bar{\boldsymbol{B}}_{\mathrm{g}} & \bar{\boldsymbol{D}}_{\mathrm{c}} & \cdots & 0 \\ \cdots & \cdots & \cdots & \cdots & \cdots \\ \bar{\boldsymbol{C}}_{\mathrm{c}}\bar{\mathbf{A}}^{N-2}\bar{\boldsymbol{B}}_{\mathrm{g}} & \bar{\boldsymbol{C}}_{\mathrm{c}}\bar{\mathbf{A}}^{N-3}\bar{\boldsymbol{B}}_{\mathrm{g}} & \bar{\boldsymbol{C}}_{\mathrm{c}}\bar{\mathbf{A}}^{N-4}\bar{\boldsymbol{B}}_{\mathrm{g}} & \cdots & \bar{\boldsymbol{D}}_{\mathrm{c}} \\ \bar{\boldsymbol{C}}_{\mathrm{c}}\bar{\mathbf{A}}^{N-1}\bar{\boldsymbol{B}}_{\mathrm{g}} & \bar{\boldsymbol{C}}_{\mathrm{c}}\bar{\mathbf{A}}^{N-2}\bar{\boldsymbol{B}}_{\mathrm{g}} & \bar{\boldsymbol{C}}_{\mathrm{c}}\bar{\mathbf{A}}^{N-3}\bar{\boldsymbol{B}}_{\mathrm{g}} & \cdots & \bar{\boldsymbol{C}}_{\mathrm{c}}\bar{\boldsymbol{B}}_{\mathrm{g}} \end{bmatrix} \tag{11}$$

$$\mathbf{Y}_{d}=\begin{bmatrix} \left(\bar{\boldsymbol{C}}_{\mathrm{c}}\mathbf{K}\right)^T & \left(\bar{\boldsymbol{C}}_{\mathrm{c}}\bar{\mathbf{A}}\mathbf{K}\right)^T & \cdots & \left(\bar{\boldsymbol{C}}_{\mathrm{c}}\bar{\mathbf{A}}^{N-1}\mathbf{K}\right)^T \end{bmatrix}^T \tag{12}$$

The previous equations are then formulated as an optimization problem in which the control input vector, $\boldsymbol{m}(k)$, is to be calculated to minimize the objective function

$$P=\min_{\boldsymbol{m}(k)}\left\{\boldsymbol{\psi}^T(k)\mathbf{Q}\boldsymbol{\psi}(k)+\Delta\boldsymbol{m}^T(k)\mathbf{R}\Delta\boldsymbol{m}(k)\right\} \tag{13}$$

subject to the following linear inequality constraints

$$\boldsymbol{m}(k)\geq\boldsymbol{m}_{\min}(k) \tag{14}$$

$$\boldsymbol{m}(k)\leq\boldsymbol{m}_{\max}(k) \tag{15}$$

$$\left|\Delta\boldsymbol{m}(k)\right|\leq\Delta\boldsymbol{m}_{\max}(k) \tag{16}$$

where $\Delta\boldsymbol{m}(k)$ is defined by

$$\Delta\boldsymbol{m}(k)=\mathbf{R}_{\Delta}\boldsymbol{m}(k)-\boldsymbol{\delta}(k) \tag{17}$$

with

$$\mathbf{R}_{\Delta}=\begin{bmatrix} \mathbf{I} & 0 & \cdots & 0 & 0 \\ -\mathbf{I} & \mathbf{I} & \cdots & 0 & 0 \\ \cdots & \cdots & \cdots & \cdots & \cdots \\ 0 & 0 & \cdots & \mathbf{I} & 0 \\ 0 & 0 & \cdots & -\mathbf{I} & \mathbf{I} \end{bmatrix} \tag{18}$$

$$\boldsymbol{\delta}(k)=\begin{bmatrix} \boldsymbol{u}^T(k-1) & 0 & \cdots & 0 \end{bmatrix}^T \tag{19}$$

Eqs. (14) ~ (15) and Eq. (16) correspond to constraints on the control surface deflections and deflection rates, respectively. The matrices **Q** and **R** in Eq. (13), which are nonnegative weighting parameters for MPC, have the following diagonal structure

$$\mathbf{Q}=\begin{bmatrix} \mathbf{Q}_0 & & & \\ & \mathbf{Q}_0 & & \\ & & \ddots & \\ & & & \mathbf{Q}_0 \end{bmatrix},\ \mathbf{R}=\begin{bmatrix} \mathbf{R}_0 & & & \\ & \mathbf{R}_0 & & \\ & & \ddots & \\ & & & \mathbf{R}_0 \end{bmatrix} \tag{20}$$

where $\mathbf{Q}_0$ and $\mathbf{R}_0$ are positive definite weighting matrices of $\bar{\boldsymbol{y}}_{\mathrm{c}}$ and $\boldsymbol{u}(k)$, respectively.

To solve the problem using standard QP methods, we define a new independent variable

$$\boldsymbol{z}(k)=\boldsymbol{m}(k)-\boldsymbol{m}_{\min}(k) \tag{21}$$

which is required to be non-negative according to Eq. (14). Then, by using the previous equations, the optimization problem can be rewritten in the following compact form such that

$$P=\min_{\boldsymbol{z}(k)} J_0=\min_{\boldsymbol{z}(k)}\left\{\tfrac{1}{2}\boldsymbol{z}^T(k)\mathbf{B}\boldsymbol{z}(k)+\boldsymbol{a}^T(k)\boldsymbol{z}(k)\right\} \tag{22}$$

subject to the constraints

$$\boldsymbol{\Phi}\boldsymbol{z}(k)\le\boldsymbol{b}(k) \tag{23}$$

where

$$\mathbf{B}=\mathbf{H}^T\mathbf{Q}\mathbf{H}+\mathbf{R}_\Delta^T\mathbf{R}\mathbf{R}_\Delta \tag{24}$$

$$\boldsymbol{a}(k)=\mathbf{H}^T\mathbf{Q}\left[\mathbf{Y}_x\hat{\boldsymbol{x}}(k\,|\,k-1)+\mathbf{Y}_v\boldsymbol{v}(k)+\mathbf{Y}_d\hat{\boldsymbol{d}}(k\,|\,k)\right]-\mathbf{R}_\Delta^T\mathbf{R}\boldsymbol{\delta}(k)+\mathbf{B}\boldsymbol{m}_{\min}(k) \tag{25}$$

$$\boldsymbol{\Phi}=\begin{bmatrix}\mathbf{I}\\ \mathbf{R}_\Delta\\ -\mathbf{R}_\Delta\end{bmatrix} \tag{26}$$

$$\boldsymbol{b}(k)=\begin{bmatrix}\boldsymbol{m}_{\max}(k)-\boldsymbol{m}_{\min}(k)\\ \Delta\boldsymbol{m}_{\max}(k)+\boldsymbol{\delta}(k)-\mathbf{R}_\Delta\boldsymbol{m}_{\min}(k)\\ \Delta\boldsymbol{m}_{\max}(k)-\boldsymbol{\delta}(k)+\mathbf{R}_\Delta\boldsymbol{m}_{\min}(k)\end{bmatrix} \tag{27}$$

The preceding QP problem can be solved efficiently using fast cone programming algorithms [34]. Note that $\boldsymbol{z}(k)\ge 0$ is a default constraint.

It is well known that for the preceding MPC problem either a small prediction horizon or control horizon may lead to unsatisfactory control performance or even closed-loop instability [27]. However, a longer prediction horizon will lead to slower transient response, and a longer control horizon will lead to larger online computation burden. These difficulties will be addressed next.

3.2 LQG based MPC

(1) Extension to infinite prediction horizon

Various techniques to ensure closed-loop stability of systems using MPC have been developed [32,35,36]. In this paper, the infinite prediction horizon technique is applied as basis for later improvement.

If the plant model is stable, the prediction horizon can be extended to infinity to ensure nominal stability. In this case, the following item J_1 should be added to J_0 in Eq. (22)

$$\begin{aligned}J_1&=\sum_{i=N+1}^{\infty}\bar{\boldsymbol{y}}_{\mathrm{c}}^{\,T}(k+i\,|\,k)\mathbf{Q}_0\bar{\boldsymbol{y}}_{\mathrm{c}}(k+i\,|\,k)\\&=\sum_{i=N}^{\infty}\bar{\boldsymbol{x}}^T(k+i\,|\,k)\bar{\boldsymbol{C}}_{\mathrm{c}}^{\,T}\mathbf{Q}_0\bar{\boldsymbol{C}}_{\mathrm{c}}\bar{\boldsymbol{x}}(k+i\,|\,k)-\bar{\boldsymbol{x}}^T(k+N\,|\,k)\bar{\boldsymbol{C}}_{\mathrm{c}}^{\,T}\mathbf{Q}_0\bar{\boldsymbol{C}}_{\mathrm{c}}\bar{\boldsymbol{x}}(k+N\,|\,k)\\&=\bar{\boldsymbol{x}}^T(k+N\,|\,k)\left[\sum_{i=0}^{\infty}\left(\bar{\mathbf{A}}^T\right)^i\bar{\boldsymbol{C}}_{\mathrm{c}}^{\,T}\mathbf{Q}_0\bar{\boldsymbol{C}}_{\mathrm{c}}\left(\bar{\mathbf{A}}\right)^i-\bar{\boldsymbol{C}}_{\mathrm{c}}^{\,T}\mathbf{Q}_0\bar{\boldsymbol{C}}_{\mathrm{c}}\right]\bar{\boldsymbol{x}}(k+N\,|\,k)\end{aligned} \tag{28}$$

Note that $w_{\mathrm{g}}(k+i)=0,\ i=N,N+1,\cdots,\infty$ is assumed. Define $\tilde{\mathbf{Q}}=\sum_{i=0}^{\infty}\left(\bar{\mathbf{A}}^T\right)^i\bar{\boldsymbol{C}}_{\mathrm{c}}^{\,T}\mathbf{Q}_0\bar{\boldsymbol{C}}_{\mathrm{c}}\left(\bar{\mathbf{A}}\right)^i$, then it is obvious that

$$\bar{\mathbf{A}}^T\tilde{\mathbf{Q}}\bar{\mathbf{A}}=\tilde{\mathbf{Q}}-\bar{\boldsymbol{C}}_{\mathrm{c}}^{\,T}\mathbf{Q}_0\bar{\boldsymbol{C}}_{\mathrm{c}} \tag{29}$$

which is a Lyapunov equation and can be solved in MATLAB by the *dlyap* function. After adding J_1 to J_0 in Eq. (22) and some matrix manipulations, the optimization problem is changed to

$$P=\min_{\boldsymbol{z}(k)}(J_0+J_1)=\min_{\boldsymbol{z}(k)}\left\{\tfrac{1}{2}\boldsymbol{z}^T(k)\tilde{\mathbf{B}}\boldsymbol{z}(k)+\tilde{\boldsymbol{a}}^T(k)\boldsymbol{z}(k)\right\} \tag{30}$$

subject to the constraints in Eq. (23) , with

$$\tilde{\mathbf{B}} = \left(\mathbf{H}^T\mathbf{Q}\mathbf{H} + \mathbf{T}\right) + \mathbf{R}_\Delta^T\mathbf{R}\mathbf{R}_\Delta \tag{31}$$

$$\begin{aligned}\tilde{\boldsymbol{a}}(k) = &\left(\mathbf{H}^T\mathbf{Q}\mathbf{Y}_{\boldsymbol{x}} + \mathbf{T}_{\boldsymbol{x}}\right)\hat{\boldsymbol{x}}(k\,|\,k-1) + \left(\mathbf{H}^T\mathbf{Q}\mathbf{Y}_{\boldsymbol{v}} + \mathbf{T}_{\boldsymbol{v}}\right)\boldsymbol{v}(k)\\ &+\left(\mathbf{H}^T\mathbf{Q}\mathbf{Y}_{\boldsymbol{d}} + \mathbf{T}_{\boldsymbol{d}}\right)\hat{\boldsymbol{d}}(k\,|\,k) - \mathbf{R}_\Delta^T\mathbf{R}\boldsymbol{\delta}(k) + \tilde{\mathbf{B}}\boldsymbol{m}_{\min}(k)\end{aligned} \tag{32}$$

where

$$\mathbf{T} = \begin{bmatrix} \bar{\boldsymbol{B}}^T\left(\bar{\mathbf{A}}^T\right)^N\tilde{\mathbf{Q}}\bar{\mathbf{A}}^N\bar{\boldsymbol{B}} & \bar{\boldsymbol{B}}^T\left(\bar{\mathbf{A}}^T\right)^N\tilde{\mathbf{Q}}\bar{\mathbf{A}}^{N-1}\bar{\boldsymbol{B}} & \cdots & \bar{\boldsymbol{B}}^T\left(\bar{\mathbf{A}}^T\right)^N\tilde{\mathbf{Q}}\bar{\mathbf{A}}\bar{\boldsymbol{B}} \\ \bar{\boldsymbol{B}}^T\left(\bar{\mathbf{A}}^T\right)^{N-1}\tilde{\mathbf{Q}}\bar{\mathbf{A}}^N\bar{\boldsymbol{B}} & \bar{\boldsymbol{B}}^T\left(\bar{\mathbf{A}}^T\right)^{N-1}\tilde{\mathbf{Q}}\bar{\mathbf{A}}^{N-1}\bar{\boldsymbol{B}} & \cdots & \bar{\boldsymbol{B}}^T\left(\bar{\mathbf{A}}^T\right)^{N-1}\tilde{\mathbf{Q}}\bar{\mathbf{A}}\bar{\boldsymbol{B}} \\ \cdots & \cdots & \cdots & \cdots \\ \bar{\boldsymbol{B}}^T\bar{\mathbf{A}}^T\tilde{\mathbf{Q}}\bar{\mathbf{A}}^N\bar{\boldsymbol{B}} & \bar{\boldsymbol{B}}^T\bar{\mathbf{A}}^T\tilde{\mathbf{Q}}\bar{\mathbf{A}}^{N-1}\bar{\boldsymbol{B}} & \cdots & \bar{\boldsymbol{B}}^T\bar{\mathbf{A}}^T\tilde{\mathbf{Q}}\bar{\mathbf{A}}\bar{\boldsymbol{B}} \end{bmatrix} \tag{33}$$

$$\mathbf{T}_{\boldsymbol{x}} = \begin{bmatrix} \left(\bar{\boldsymbol{B}}^T\left(\bar{\mathbf{A}}^T\right)^N\tilde{\mathbf{Q}}\bar{\mathbf{A}}^{N+1}\right)^T & \left(\bar{\boldsymbol{B}}^T\left(\bar{\mathbf{A}}^T\right)^{N-1}\tilde{\mathbf{Q}}\bar{\mathbf{A}}^{N+1}\right)^T & \cdots & \left(\bar{\boldsymbol{B}}^T\bar{\mathbf{A}}^T\tilde{\mathbf{Q}}\bar{\mathbf{A}}^{N+1}\right)^T \end{bmatrix}^T \tag{34}$$

$$\mathbf{T}_{\boldsymbol{v}} = \begin{bmatrix} \bar{\boldsymbol{B}}^T\left(\bar{\mathbf{A}}^T\right)^N\tilde{\mathbf{Q}}\bar{\mathbf{A}}^N\bar{\boldsymbol{B}}_{\mathrm{g}} & \bar{\boldsymbol{B}}^T\left(\bar{\mathbf{A}}^T\right)^N\tilde{\mathbf{Q}}\bar{\mathbf{A}}^{N-1}\bar{\boldsymbol{B}}_{\mathrm{g}} & \cdots & \bar{\boldsymbol{B}}^T\left(\bar{\mathbf{A}}^T\right)^N\tilde{\mathbf{Q}}\bar{\mathbf{A}}\bar{\boldsymbol{B}}_{\mathrm{g}} \\ \bar{\boldsymbol{B}}^T\left(\bar{\mathbf{A}}^T\right)^{N-1}\tilde{\mathbf{Q}}\bar{\mathbf{A}}^N\bar{\boldsymbol{B}}_{\mathrm{g}} & \bar{\boldsymbol{B}}^T\left(\bar{\mathbf{A}}^T\right)^{N-1}\tilde{\mathbf{Q}}\bar{\mathbf{A}}^{N-1}\bar{\boldsymbol{B}}_{\mathrm{g}} & \cdots & \bar{\boldsymbol{B}}^T\left(\bar{\mathbf{A}}^T\right)^{N-1}\tilde{\mathbf{Q}}\bar{\mathbf{A}}\bar{\boldsymbol{B}}_{\mathrm{g}} \\ \cdots & \cdots & \cdots & \cdots \\ \bar{\boldsymbol{B}}^T\bar{\mathbf{A}}^T\tilde{\mathbf{Q}}\bar{\mathbf{A}}^N\bar{\boldsymbol{B}}_{\mathrm{g}} & \bar{\boldsymbol{B}}^T\bar{\mathbf{A}}^T\tilde{\mathbf{Q}}\bar{\mathbf{A}}^{N-1}\bar{\boldsymbol{B}}_{\mathrm{g}} & \cdots & \bar{\boldsymbol{B}}^T\bar{\mathbf{A}}^T\tilde{\mathbf{Q}}\bar{\mathbf{A}}\bar{\boldsymbol{B}}_{\mathrm{g}} \end{bmatrix} \tag{35}$$

$$\mathbf{T}_{\boldsymbol{d}} = \begin{bmatrix} \left(\bar{\boldsymbol{B}}^T\left(\bar{\mathbf{A}}^T\right)^N\tilde{\mathbf{Q}}\bar{\mathbf{A}}^N\mathbf{K}\right)^T & \left(\bar{\boldsymbol{B}}^T\left(\bar{\mathbf{A}}^T\right)^{N-1}\tilde{\mathbf{Q}}\bar{\mathbf{A}}^N\mathbf{K}\right)^T & \cdots & \left(\bar{\boldsymbol{B}}^T\bar{\mathbf{A}}^T\tilde{\mathbf{Q}}\bar{\mathbf{A}}^N\mathbf{K}\right)^T \end{bmatrix}^T \tag{36}$$

Since this MPC method is characterized by infinite prediction horizon, it will be denoted as MPC_IH in the following discussions.

Remark 1: Through application of infinite prediction horizon, nominal stability of the MPC controller is guaranteed. However, the addition of J_1 in Eq. (30) reduces the influence of J_0 on the optimization problem, which may cause an increase of J_0 compared to the open-loop case as long as the sum of J_0 and J_1 is minimized through optimization. In other words, this method may lead to overshoot of the controlled output $\boldsymbol{y}_c$.

(2) Extension to infinite control horizon through using LQG controller

Two methods are available to improve the control performance of the MPC_IH controller. The first approach is to reduce the effect of J_1 on P in Eq. (30) through multiplying J_1 by a coefficient r less than 1. This method corresponds to increasing the weight of $\bar{\boldsymbol{y}}_{\mathrm{c}}(k+i\,|\,k), i=1,2,\cdots,N$ in the objective function P; but a new problem is then posed since the optimal value of r is found to be strongly dependent on the gust scale, gust amplitude and the flight condition. The second approach is to extend the control horizon N, but this will lead to an increase of the online computation burden, which is particularly serious for high-order systems.

Based on the previous discussions, this paper proposed an improved scheme which extends the control horizon to infinity without increasing the computation burden. This goal is realized through introducing linear quadratic (LQ) infinite optimal control into the MPC frame. Specifically, it is supposed in the QP problem that after the first N control moves, state feedback control is applied for GLA. The states used for feedback control are estimated by the Kalman filter, i.e.

$$\boldsymbol{u}(k+i\,|\,k) = \mathbf{K}_{\mathrm{r}}\bar{\boldsymbol{x}}(k+i\,|\,k),\ i=N, N+1,\cdots,\infty \tag{37}$$

where $\mathbf{K}_{\mathrm{r}}$ is the feedback gain of the LQ controller. If $\mathbf{K}_{\mathrm{r}}$ is designed offline, the QP problem solved at each sampling time will have the same dimension as before since the optimized variables are still $\boldsymbol{u}(k+i\,|\,k), i=0,1,\cdots,N-1$. Therefore, the online computation burden is not increased. Through

a properly designed LQ controller, the convergence rate of $\bar{\boldsymbol{y}}_{\mathrm{c}}(k+i\,|\,k), i=N, N+1, \cdots, \infty$ will be faster, which then leads to the reduction of J_1 in Eq. (30). This approach is similar to the application of the coefficient r discussed before, but the challenge now becomes design of the LQ controller.

It should be noticed that the control efforts in Eq. (37) are not considered in the performance function in Eq. (30) since these are fictitious inputs with much less importance than $\bar{\boldsymbol{y}}_{\mathrm{c}}(k+i\,|\,k), i=1,\ 2, \cdots, \infty$ and $\boldsymbol{u}(k+i\,|\,k), i=0, 1, \cdots, N-1$. Actually, through numerical examples it is found that adding these control efforts to the performance function indeed makes no difference to the control results.

Remark 2: Before we proceed to the design method of the LQ controller, an important aspect of the current MPC formulation should be clarified. It may seem unreasonable that LQ control is not considered for the first N steps in the algorithm. In that case, the state feedback structure of the LQ controller will be destroyed when independent variables are added to the control inputs. Due to the optimality of the solutions, the optimized control sequence will be the same whether the LQ control is included in the first N steps or not. Therefore, the proposed MPC formulation is actually an integrated combination of the traditional MPC and LQ control. Obviously, it is also a combined feedforward-feedback approach.

In addition, the coupling between the Kalman filter and the LQ controller should be considered, since the performance of the LQ controller is dependent on the estimation accuracy of the Kalman filter and this coupling directly affects the system stability margin. Therefore, a simultaneous design of the Kalman filter and the LQ controller is necessary and a successful design should contribute to better control performance and stability property. Since the combination of the LQ controller and the Kalman filter is a LQG controller, the current demand is for a well-designed LQG controller. Fortunately, an improved LQG method for GLA has been proposed by the authors before [29]. Through introduction of fictitious high-frequency noise in the design phase, this improved LQG method is proved to have enough robust performance and robust stability around the design point. Details about this algorithm are not introduced here for simplicity, and the feedback gain of the LQ controller $\mathbf{K}_{\mathrm{r}}$ and the Kalman filter gain $\mathbf{K}$ are treated as known values in this paper.

Remark 3: Since LQG control is an unconstrained control design method, it is difficult to enforce constraints on the control input in Eq. (37), i.e., $\boldsymbol{u}(k+i\,|\,k),\ i=N, N+1, \cdots, \infty$. A common solution is to adjust N so that, after N control moves, the system states enter a terminal state region, in which the input constraints are always satisfied. Apparently, the minimum value of N is then dependent on the current system states, the state estimation error, the measured gust signal and input constraints. That is to say, to strictly guarantee satisfaction of constraints on the control input in Eq. (37), it is necessary to decide the value of N before solving the QP problem, which greatly increases the problem complexity and computation burden. In view of this, a simpler method is applied in this paper. Specifically, constraints on the control input in Eq. (37) are only considered in the LQG design process through time domain simulations for a family of discrete gust profiles specified by relevant regulations (details will be given in Section 4). In principle, this method is equivalent to relaxing the constraints on the control input in Eq. (37). Reasonability of this method will be further verified in Section 4.

It can be easily observed that the application of the LQ controller changes J_1 in Eq. (28) through replacing $\bar{\mathbf{A}}$ with

$$\hat{\mathbf{A}} = \bar{\mathbf{A}} + \bar{\mathbf{B}}\mathbf{K}_{\mathrm{r}} \tag{38}$$

Consequently, $\tilde{\mathbf{Q}}$ in Eq. (29) is replaced with $\hat{\mathbf{Q}}$ solved by the Lyapunov equation

$$\left(\hat{\mathbf{A}}\right)^{T} \hat{\mathbf{Q}}\hat{\mathbf{A}} = \hat{\mathbf{Q}} - \bar{\boldsymbol{C}}_{\mathrm{c}}{}^{T}\mathbf{Q}_0\bar{\boldsymbol{C}}_{\mathrm{c}} \tag{39}$$

and therefore, the only difference between the current MPC formulation and the MPC_IH formulation

is that the matrix $\tilde{\mathbf{Q}}$ in Eq. (33) ~ (36) is replaced with $\hat{\mathbf{Q}}$.

Considering the structure of the new formulation, it will be denoted as MPC_LQG in the following discussions.

There are two main differences between the MPC_LQG formulation and the previous MPC_IH formulation. Firstly, the MPC_LQG formulation adopts infinite control horizon through application of the LQ controller. Specifically, the infinite control signal sequence is divided into two parts. The forepart consists of a limited number of online optimized variables which are similar to $\boldsymbol{m}(k)$ in Section 3.1, and the second part is output of the offline designed LQ controller, which receives states information of the plant estimated by the Kalman filter. This approach helps to alleviate the problem in Remark 1 since the value of J_1 in Eq. (30) is effectively reduced through the LQ controller. Secondly, the MPC_LQG formulation is applicable to open-loop unstable plant as long as it can be stabilized by the LQG controller, which enlarges the application scope of the previous MPC_IH method.

Remark 4: For the MPC_LQG formulation, the introduction of the LQ controller also helps to reduce the control burden in the first N sampling periods. Compared to the MPC_IH method using an infinite prediction horizon, the new controller is less likely to reach saturation. Furthermore, better performance of the new algorithm also provides the possibility of reducing the dimension of the optimization problem through reducing N. This will be verified in Section 4.

(3) Method to deal with control delay

The large online computation burden has been the key barrier that keeps the MPC techniques from being applied to systems with large order and fast dynamics, although this problem may be alleviated by certain model reduction techniques, better computer hardware and superior QP algorithms. The online computation time leads to control delay which is usually adverse to control performance. Besides, digital/analog conversions and noise filters are also origins of control delay [37]. In this subsection, a method to deal with control delay is proposed. The novelty of this method lies in the following two aspects. First, at each sampling time k, the control sequence being optimized now begins with $\boldsymbol{u}(k+d_{\mathrm{u}}\,|\,k)$ instead of $\boldsymbol{u}(k\,|\,k)$, where d_{u} is an integer defining the maximal control delay. This means that the control inputs being optimized will be applied after d_{u} sampling periods instead of at the current sampling period, which effectively compensates for the control delay caused by the computation time and other factors. Second, the first d_{u} elements of the optimal solution are applied instead of only the first one, which can be described by

$$\boldsymbol{u}(k+d_{\mathrm{u}}+i)=\boldsymbol{u}(k+d_{\mathrm{u}}+i\,|\,k),\ i=0,1,\cdots,d_{\mathrm{u}}-1 \tag{40}$$

The control strategy can be explained by Fig. 2, where d_{u} is supposed to be 4. At sampling time k_1, the optimized control sequence is $\boldsymbol{u}(k_2+i\,|\,k_1),\ i=0,1,\cdots,N-1$ and the first d_{u} elements are applied. Similarly, at sampling time k_2, the optimized control sequence is $\boldsymbol{u}(k_3+i\,|\,k_2),\ i=0,1,\cdots,N-1$ and the first d_{u} elements are applied. Note that $N\geq d_{\mathrm{u}}$ must be satisfied, where N is no longer the control horizon, but the number of optimized free control moves. Furthermore, the initial control sequence is $\boldsymbol{u}(k)=0,\ k=1,2,\cdots,d_{\mathrm{u}}$. It can be easily concluded that the QP optimization problem is solved every d_{u} sampling steps instead of every sampling step.

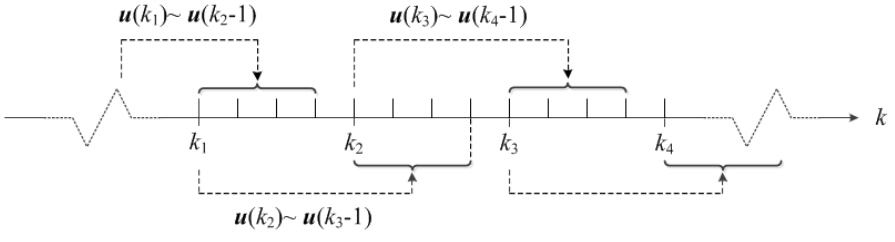

Fig. 2. Schematic diagram of the control strategy

At sampling time k, the known control inputs that will be executed are denoted as

$$\begin{aligned}\boldsymbol{m}_0(k) &= \left[\boldsymbol{u}^T(k) \quad \boldsymbol{u}^T(k+1) \quad \cdots \quad \boldsymbol{u}^T(k+d_{\mathrm{u}}-1)\right]^T \\ &= \left[\boldsymbol{u}^T(k\,|\,k-d_{\mathrm{u}}) \quad \boldsymbol{u}^T(k+1\,|\,k-d_{\mathrm{u}}) \quad \cdots \quad \boldsymbol{u}^T(k+d_{\mathrm{u}}-1\,|\,k-d_{\mathrm{u}})\right]^T\end{aligned} \tag{41}$$

and the optimized future control inputs are

$$\boldsymbol{m}(k) = \left[\boldsymbol{u}^T(k+d_{\mathrm{u}}\,|\,k) \quad \boldsymbol{u}^T(k+d_{\mathrm{u}}+1\,|\,k) \quad \cdots \quad \boldsymbol{u}^T(k+d_{\mathrm{u}}+N-1\,|\,k)\right]^T \tag{42}$$

Accordingly, Eq. (19) is changed to

$$\boldsymbol{\delta}(k) = \left[\boldsymbol{u}^T(k+d_{\mathrm{u}}-1) \quad 0 \quad \cdots \quad 0\right]^T \tag{43}$$

Considering Eq. (41) and Eq. (42), Eq. (8) is changed to

$$\boldsymbol{v}(k) = \left[w_{\mathrm{g}}(k) \quad w_{\mathrm{g}}(k+1) \quad \cdots \quad w_{\mathrm{g}}(k+N+d_{\mathrm{u}}-1)\right] \tag{44}$$

Note that if the lead time of the LIDAR system or the alpha probe can't cover the scope of $\boldsymbol{v}(k)$ in Eq. (44), the unmeasured part of $\boldsymbol{v}(k)$ should be filled with zeros.

Using the transformation in Eq. (21) and some matrix manipulations, the QP optimization problem is changed to

$$P = \min_{\boldsymbol{z}(k)} \left\{ \tfrac{1}{2}\boldsymbol{z}^T(k)\hat{\mathbf{B}}\boldsymbol{z}(k) + \hat{\boldsymbol{a}}^T(k)\boldsymbol{z}(k) \right\} \tag{45}$$

subject to the constraints in Eq. (23), where

$$\hat{\mathbf{B}} = \left(\mathbf{H}^T\mathbf{Q}\mathbf{H} + \hat{\mathbf{T}}\right) + \mathbf{R}_{\Delta}^T\mathbf{R}\mathbf{R}_{\Delta} \tag{46}$$

$$\begin{aligned}\hat{\boldsymbol{a}}(k) = &\left(\mathbf{H}^T\mathbf{Q}\mathbf{H}_{\boldsymbol{m}_0} + \hat{\mathbf{T}}_{\boldsymbol{m}_0}\right)\boldsymbol{m}_0 + \left(\mathbf{H}^T\mathbf{Q}\hat{\mathbf{Y}}_{\boldsymbol{x}} + \hat{\mathbf{T}}_{\boldsymbol{x}}\right)\hat{\boldsymbol{x}}(k\,|\,k-1) + \left(\mathbf{H}^T\mathbf{Q}\hat{\mathbf{Y}}_{\boldsymbol{v}} + \hat{\mathbf{T}}_{\boldsymbol{v}}\right)\boldsymbol{v}(k) \\ &+ \left(\mathbf{H}^T\mathbf{Q}\hat{\mathbf{Y}}_{\boldsymbol{d}} + \hat{\mathbf{T}}_{\boldsymbol{d}}\right)\hat{\boldsymbol{d}}(k\,|\,k) - \mathbf{R}_{\Delta}^T\mathbf{R}\boldsymbol{\delta}(k) + \hat{\mathbf{B}}\boldsymbol{m}_{\min}(k)\end{aligned} \tag{47}$$

and

$$\mathbf{H}_{\boldsymbol{m}_0} = \begin{bmatrix} \bar{\boldsymbol{C}}_{\mathrm{c}}\bar{\mathbf{A}}^{d_u}\bar{\boldsymbol{B}} & \bar{\boldsymbol{C}}_{\mathrm{c}}\bar{\mathbf{A}}^{d_u-1}\bar{\boldsymbol{B}} & \cdots & \bar{\boldsymbol{C}}_{\mathrm{c}}\bar{\mathbf{A}}\bar{\boldsymbol{B}} \\ \bar{\boldsymbol{C}}_{\mathrm{c}}\bar{\mathbf{A}}^{d_u+1}\bar{\boldsymbol{B}} & \bar{\boldsymbol{C}}_{\mathrm{c}}\bar{\mathbf{A}}^{d_u}\bar{\boldsymbol{B}} & \cdots & \bar{\boldsymbol{C}}_{\mathrm{c}}\bar{\mathbf{A}}^{2}\bar{\boldsymbol{B}} \\ \cdots & \cdots & \cdots & \cdots \\ \bar{\boldsymbol{C}}_{\mathrm{c}}\bar{\mathbf{A}}^{N+d_u-1}\bar{\boldsymbol{B}} & \bar{\boldsymbol{C}}_{\mathrm{c}}\bar{\mathbf{A}}^{N+d_u-2}\bar{\boldsymbol{B}} & \cdots & \bar{\boldsymbol{C}}_{\mathrm{c}}\bar{\mathbf{A}}^{N}\bar{\boldsymbol{B}} \end{bmatrix} \tag{48}$$

$$\hat{\mathbf{Y}}_{\boldsymbol{x}} = \left[\left(\bar{\boldsymbol{C}}_{\mathrm{c}}\bar{\mathbf{A}}^{d_u+1}\right)^T \quad \left(\bar{\boldsymbol{C}}_{\mathrm{c}}\bar{\mathbf{A}}^{d_u+2}\right)^T \quad \cdots \quad \left(\bar{\boldsymbol{C}}_{\mathrm{c}}\bar{\mathbf{A}}^{d_u+N}\right)^T\right]^T \tag{49}$$

$$\hat{\mathbf{Y}}_{\boldsymbol{v}} = \begin{bmatrix} \bar{\boldsymbol{C}}_{\mathrm{c}}\bar{\mathbf{A}}^{d_u}\bar{\boldsymbol{B}}_{\mathrm{g}} & \bar{\boldsymbol{C}}_{\mathrm{c}}\bar{\mathbf{A}}^{d_u-1}\bar{\boldsymbol{B}}_{\mathrm{g}} & \cdots & \bar{\boldsymbol{C}}_{\mathrm{c}}\bar{\boldsymbol{B}}_{\mathrm{g}} & \bar{\boldsymbol{D}}_{\mathrm{c}} & 0 & \cdots & 0 \\ \bar{\boldsymbol{C}}_{\mathrm{c}}\bar{\mathbf{A}}^{d_u+1}\bar{\boldsymbol{B}}_{\mathrm{g}} & \bar{\boldsymbol{C}}_{\mathrm{c}}\bar{\mathbf{A}}^{d_u}\bar{\boldsymbol{B}}_{\mathrm{g}} & \cdots & \cdots & \bar{\boldsymbol{C}}_{\mathrm{c}}\bar{\boldsymbol{B}}_{\mathrm{g}} & \bar{\boldsymbol{D}}_{\mathrm{c}} & \cdots & 0 \\ \cdots & \cdots & \cdots & \cdots & \cdots & \cdots & \cdots & \cdots \\ \bar{\boldsymbol{C}}_{\mathrm{c}}\bar{\mathbf{A}}^{N+d_u-2}\bar{\boldsymbol{B}}_{\mathrm{g}} & \bar{\boldsymbol{C}}_{\mathrm{c}}\bar{\mathbf{A}}^{N+d_u-3}\bar{\boldsymbol{B}}_{\mathrm{g}} & \cdots & \cdots & \cdots & \cdots & \cdots & \bar{\boldsymbol{D}}_{\mathrm{c}} \\ \bar{\boldsymbol{C}}_{\mathrm{c}}\bar{\mathbf{A}}^{N+d_u-1}\bar{\boldsymbol{B}}_{\mathrm{g}} & \bar{\boldsymbol{C}}_{\mathrm{c}}\bar{\mathbf{A}}^{N+d_u-2}\bar{\boldsymbol{B}}_{\mathrm{g}} & \cdots & \cdots & \cdots & \cdots & \cdots & \bar{\boldsymbol{C}}_{\mathrm{c}}\bar{\boldsymbol{B}}_{\mathrm{g}} \end{bmatrix} \tag{50}$$

$$\hat{\mathbf{Y}}_{\boldsymbol{d}} = \left[\left(\bar{\boldsymbol{C}}_{\mathrm{c}}\bar{\mathbf{A}}^{d_u}\mathbf{K}\right)^T \quad \left(\bar{\boldsymbol{C}}_{\mathrm{c}}\bar{\mathbf{A}}^{d_u+1}\mathbf{K}\right)^T \quad \cdots \quad \left(\bar{\boldsymbol{C}}_{\mathrm{c}}\bar{\mathbf{A}}^{N+d_u-1}\mathbf{K}\right)^T\right]^T \tag{51}$$

$$\hat{\mathbf{T}} = \begin{bmatrix} \bar{\boldsymbol{B}}^T\left(\bar{\mathbf{A}}^T\right)^N\hat{\mathbf{Q}}\bar{\mathbf{A}}^N\bar{\boldsymbol{B}} & \bar{\boldsymbol{B}}^T\left(\bar{\mathbf{A}}^T\right)^N\hat{\mathbf{Q}}\bar{\mathbf{A}}^{N-1}\bar{\boldsymbol{B}} & \cdots & \bar{\boldsymbol{B}}^T\left(\bar{\mathbf{A}}^T\right)^N\hat{\mathbf{Q}}\bar{\mathbf{A}}\bar{\boldsymbol{B}} \\ \bar{\boldsymbol{B}}^T\left(\bar{\mathbf{A}}^T\right)^{N-1}\hat{\mathbf{Q}}\bar{\mathbf{A}}^N\bar{\boldsymbol{B}} & \bar{\boldsymbol{B}}^T\left(\bar{\mathbf{A}}^T\right)^{N-1}\hat{\mathbf{Q}}\bar{\mathbf{A}}^{N-1}\bar{\boldsymbol{B}} & \cdots & \bar{\boldsymbol{B}}^T\left(\bar{\mathbf{A}}^T\right)^{N-1}\hat{\mathbf{Q}}\bar{\mathbf{A}}\bar{\boldsymbol{B}} \\ \cdots & \cdots & \cdots & \cdots \\ \bar{\boldsymbol{B}}^T\bar{\mathbf{A}}^T\hat{\mathbf{Q}}\bar{\mathbf{A}}^N\bar{\boldsymbol{B}} & \bar{\boldsymbol{B}}^T\bar{\mathbf{A}}^T\hat{\mathbf{Q}}\bar{\mathbf{A}}^{N-1}\bar{\boldsymbol{B}} & \cdots & \bar{\boldsymbol{B}}^T\bar{\mathbf{A}}^T\hat{\mathbf{Q}}\bar{\mathbf{A}}\bar{\boldsymbol{B}} \end{bmatrix} \tag{52}$$

$$\hat{\mathbf{T}}_{m_0}=\begin{bmatrix} \bar{\boldsymbol{B}}^T\left(\bar{\mathbf{A}}^T\right)^N\hat{\mathbf{Q}}\bar{\mathbf{A}}^{N+d_u}\bar{\boldsymbol{B}} & \bar{\boldsymbol{B}}^T\left(\bar{\mathbf{A}}^T\right)^N\hat{\mathbf{Q}}\bar{\mathbf{A}}^{N+d_u-1}\bar{\boldsymbol{B}} & \cdots & \bar{\boldsymbol{B}}^T\left(\bar{\mathbf{A}}^T\right)^N\hat{\mathbf{Q}}\bar{\mathbf{A}}^{N+1}\bar{\boldsymbol{B}} \\ \bar{\boldsymbol{B}}^T\left(\bar{\mathbf{A}}^T\right)^{N-1}\hat{\mathbf{Q}}\bar{\mathbf{A}}^{N+d_u}\bar{\boldsymbol{B}} & \bar{\boldsymbol{B}}^T\left(\bar{\mathbf{A}}^T\right)^{N-1}\hat{\mathbf{Q}}\bar{\mathbf{A}}^{N+d_u-1}\bar{\boldsymbol{B}} & \cdots & \bar{\boldsymbol{B}}^T\left(\bar{\mathbf{A}}^T\right)^{N-1}\hat{\mathbf{Q}}\bar{\mathbf{A}}^{N+1}\bar{\boldsymbol{B}} \\ \cdots & \cdots & \cdots & \cdots \\ \bar{\boldsymbol{B}}^T\bar{\mathbf{A}}^T\hat{\mathbf{Q}}\bar{\mathbf{A}}^{N+d_u}\bar{\boldsymbol{B}} & \bar{\boldsymbol{B}}^T\bar{\mathbf{A}}^T\hat{\mathbf{Q}}\bar{\mathbf{A}}^{N+d_u-1}\bar{\boldsymbol{B}} & \cdots & \bar{\boldsymbol{B}}^T\bar{\mathbf{A}}^T\hat{\mathbf{Q}}\bar{\mathbf{A}}^{N+1}\bar{\boldsymbol{B}} \end{bmatrix} \tag{53}$$

$$\hat{\mathbf{T}}_x=\begin{bmatrix}\left(\bar{\boldsymbol{B}}^T\left(\bar{\mathbf{A}}^T\right)^N\tilde{\mathbf{Q}}\bar{\mathbf{A}}^{N+d_u+1}\right)^T & \left(\bar{\boldsymbol{B}}^T\left(\bar{\mathbf{A}}^T\right)^{N-1}\tilde{\mathbf{Q}}\bar{\mathbf{A}}^{N+d_u+1}\right)^T & \cdots & \left(\bar{\boldsymbol{B}}^T\bar{\mathbf{A}}^T\tilde{\mathbf{Q}}\bar{\mathbf{A}}^{N+d_u+1}\right)^T\end{bmatrix}^T \tag{54}$$

$$\hat{\mathbf{T}}_v=\begin{bmatrix} \bar{\boldsymbol{B}}^T\left(\bar{\mathbf{A}}^T\right)^N\hat{\mathbf{Q}}\bar{\mathbf{A}}^{N+d_u}\bar{\boldsymbol{B}}_g & \bar{\boldsymbol{B}}^T\left(\bar{\mathbf{A}}^T\right)^N\hat{\mathbf{Q}}\bar{\mathbf{A}}^{N+d_u-1}\bar{\boldsymbol{B}}_g & \cdots & \bar{\boldsymbol{B}}^T\left(\bar{\mathbf{A}}^T\right)^N\hat{\mathbf{Q}}\bar{\mathbf{A}}\bar{\boldsymbol{B}}_g \\ \bar{\boldsymbol{B}}^T\left(\bar{\mathbf{A}}^T\right)^{N-1}\hat{\mathbf{Q}}\bar{\mathbf{A}}^{N+d_u}\bar{\boldsymbol{B}}_g & \bar{\boldsymbol{B}}^T\left(\bar{\mathbf{A}}^T\right)^{N-1}\hat{\mathbf{Q}}\bar{\mathbf{A}}^{N+d_u-1}\bar{\boldsymbol{B}}_g & \cdots & \bar{\boldsymbol{B}}^T\left(\bar{\mathbf{A}}^T\right)^{N-1}\hat{\mathbf{Q}}\bar{\mathbf{A}}\bar{\boldsymbol{B}}_g \\ \cdots & \cdots & \cdots & \cdots \\ \bar{\boldsymbol{B}}^T\bar{\mathbf{A}}^T\hat{\mathbf{Q}}\bar{\mathbf{A}}^{N+d_u}\bar{\boldsymbol{B}}_g & \bar{\boldsymbol{B}}^T\bar{\mathbf{A}}^T\hat{\mathbf{Q}}\bar{\mathbf{A}}^{N+d_u-1}\bar{\boldsymbol{B}}_g & \cdots & \bar{\boldsymbol{B}}^T\bar{\mathbf{A}}^T\hat{\mathbf{Q}}\bar{\mathbf{A}}\bar{\boldsymbol{B}}_g \end{bmatrix} \tag{55}$$

$$\hat{\mathbf{T}}_d=\begin{bmatrix}\left(\bar{\boldsymbol{B}}^T\left(\bar{\mathbf{A}}^T\right)^N\hat{\mathbf{Q}}\bar{\mathbf{A}}^{N+d_u}\mathbf{K}\right)^T & \left(\bar{\boldsymbol{B}}^T\left(\bar{\mathbf{A}}^T\right)^{N-1}\hat{\mathbf{Q}}\bar{\mathbf{A}}^{N+d_u}\mathbf{K}\right)^T & \cdots & \left(\bar{\boldsymbol{B}}^T\bar{\mathbf{A}}^T\hat{\mathbf{Q}}\bar{\mathbf{A}}^{N+d_u}\mathbf{K}\right)^T\end{bmatrix}^T \tag{56}$$

The effectiveness of this technique will be verified in Section 4.

4. Numerical Examples

4.1 Model description and open-loop dynamics

Numerical results on a general transport aircraft model shown in Fig. 3 are now used to demonstrate the effectiveness and advantages of the MPC_LQG approach. The aircraft weight is 7203.7 kg. The length and the height of the aircraft are 22.0 m and 6.0 m, respectively. The gust is measured by the alpha probe at the aircraft's nose, which is 7.0 m ahead of the wing. Only the longitudinal dynamics are considered and nine symmetric modes are used to construct the aeroelastic model, including the rigid plunge and pitch modes. Descriptions of the structural modes are given in Table 1. More detailed descriptions of the aircraft model can be found in [38].

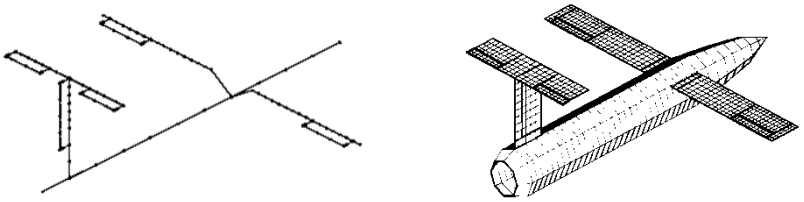

(a) Structural model (b) Aerodynamic model

Fig. 3. Model of the general transport aircraft

One pair of symmetric actuated ailerons and elevators are taken as control inputs. The transfer functions of the actuators are

$$G_{ac}=\frac{3.302\times10^5}{s^3+127.2s^2+8789s+3.302\times10^5} \tag{57}$$

The sensor output consists of the vertical acceleration of the wing tip acceleration, the center of gravity (c.g.) and the aircraft pitch rate. The controlled output includes the wing root bending moment, the c.g. acceleration and the aircraft pitch rate. In addition, the sampling time of the discretion model is 5 ms. The objective of the GLA system is to reduce the wing root bending moment, the c.g. acceleration and the aircraft pitch rate while keeping the wing root torsional moment monitored. The c.g. acceleration and the aircraft pitch rate are alleviated for ride quality improvement. Meanwhile, the control surface deflections and deflection rates are limited to be less than 8 degrees and 100 degrees/s, respectively.

Table 1. Descriptions of structural modes

	Frequency (Hz)	Modal description
1	0.0	Plunge mode
2	0.0	Pitch mode
3	7.96	First symmetrical bending mode of the wing
4	13.96	First symmetrical bending mode of the horizontal
5	17.45	First symmetrical torsional mode of the wing
6	26.28	Second symmetrical bending mode of the wing
7	32.47	Vertical first bending mode of the fuselage
8	37.92	First symmetrical torsional mode of the horizontal
9	41.11	Second symmetrical torsional mode of the wing

The nominal flight condition is set to M = 0.4 and H = 5 km with standard atmosphere assumed. A family of discrete '1-cos' gusts is considered as

$$w_{\mathrm{g}} = \begin{cases} \dfrac{1}{2} w_{\mathrm{gm}} \left(1 - \cos\left(\dfrac{\pi s}{L_{\mathrm{g}}} \right) \right) & 0 < s \le 2L_{\mathrm{g}} \\ 0 & s > 2L_{\mathrm{g}} \end{cases} \tag{58}$$

where L_{g} is the half of the gust length, s is the distance into the gust disturbance and w_{gm} is the peak gust velocity determined through the EASA regulations [39]. These gust profiles and the corresponding open-loop responses of the wing root bending moment are shown in Fig. 4. It is observed that the worst discrete gust corresponds to the case L_{g} = 9 m, which leads to the largest wing root bending moment. Therefore, the discrete gust corresponds to the case L_{g} = 9 m is studied in the following discussions unless otherwise stated.

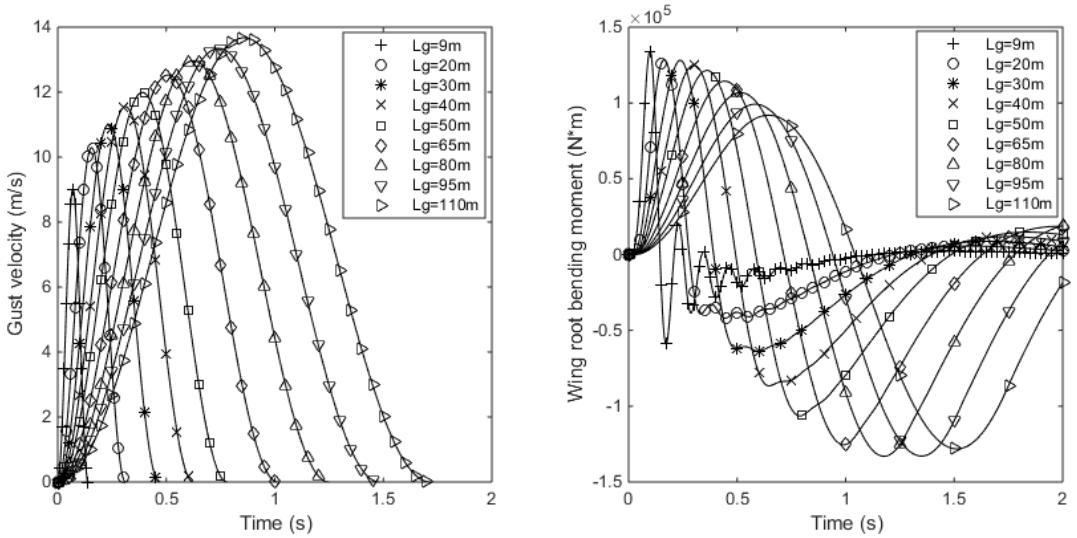

Fig. 4. A series of 1-cos gust inputs (left) and the corresponding wing root bending moment (right).

4.2 Nominal closed-loop control performance

Regarding the objective function of the MPC algorithm, the weighting matrices in Eq. (20) are set as $\mathbf{Q}_0 = \mathbf{I}$ and $\mathbf{R}_0 = 300\mathbf{I}$ after all the controlled outputs are normalized by their maximal values during the worst case discrete gust excitation. The purpose of assigning large value to $\mathbf{R}_0$ is to suppress the small amplitude oscillation of control surfaces, especially when control delay is considered. The QP problems are solved by the *quadprog* command in Matlab at each sampling time.

When the flight parameters of the internal model are same as those of the plant model, the GLA

results from different controllers for the worst discrete gust are shown in Fig. 5~10, where all the outputs are normalized by the corresponding maximal open-loop responses. In Fig. 5~6, the control results of the LQG controller and the traditional MPC controller, with $N = 30$, are shown respectively. Note that the LQG controller is designed using the method in [29] with two constraints considered: the first is that the control saturation must not be reached for all the gust cases in Fig. 4; the second is that the closed-loop stability should be ensured as the Mach number varying between 0.3 and 0.5, while the flight height is fixed to H = 5 km. Through comparing Fig. 5 and Fig. 6, the traditional MPC controller is found to present better performance than the LQG controller due to larger control surface deflections. It should be mentioned that for the traditional MPC controller, choosing $N = 10$ instead of $N = 30$ will lead to the closed-loop system instability. But increase of N will cause higher computation burden at each sampling time.

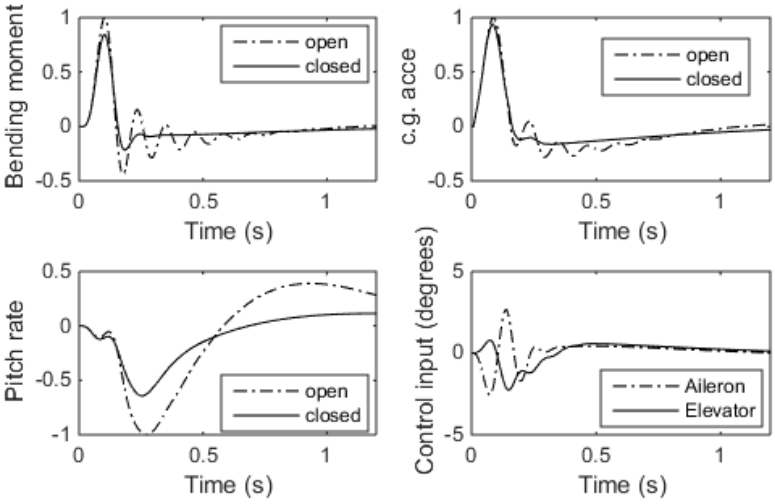

Fig. 5. Control performance of the LQG controller

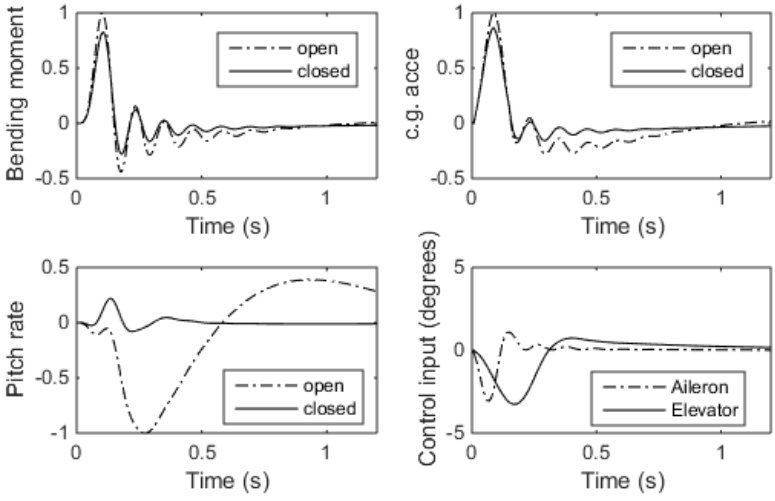

Fig. 6. Control performance of the traditional MPC controller ($N = 30$)

In Fig. 7, the control results of the MPC_IH controller are shown. It is obvious that control saturation occurs and this saturation causes adverse output responses after the first peak, which confirms the discussion in Remark 1. In Fig. 8, control results of the MPC_LQG controller are depicted, where $d_u = 0$ means that control delay is not considered. With $N = 10$, the system is well controlled and the GLA performance is superior to all the above results in Figs. 5~7. Furthermore, the control saturation is eliminated compared to Fig. 7. Fig. 9 presents the bending-torsion diagram of wing root for each controller. The MPC_LQG controller is found to slightly increase the wing root torsional

moment, which is acceptable but should be considered in structural design.

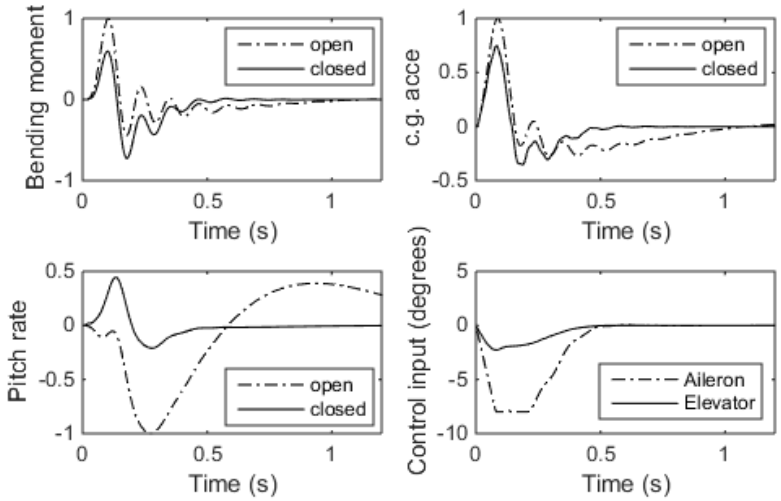

Fig. 7. Control performance of the MPC_IH controller (N = 10)

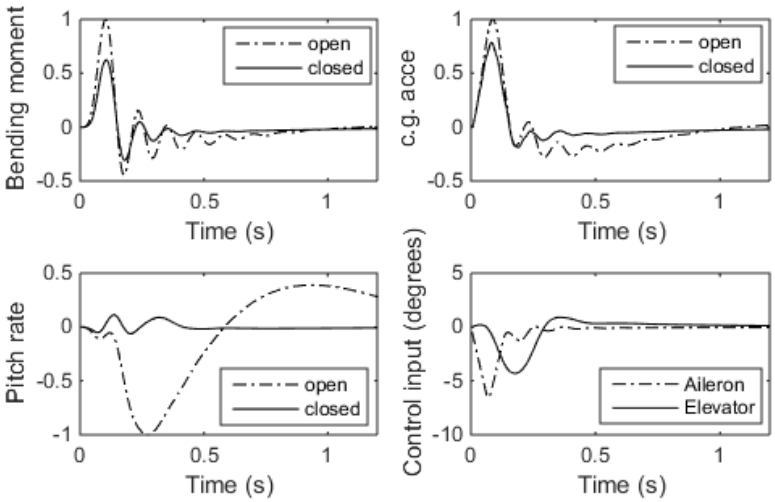

Fig. 8. Control performance of the MPC_LQG controller (N = 10, d_u = 0)

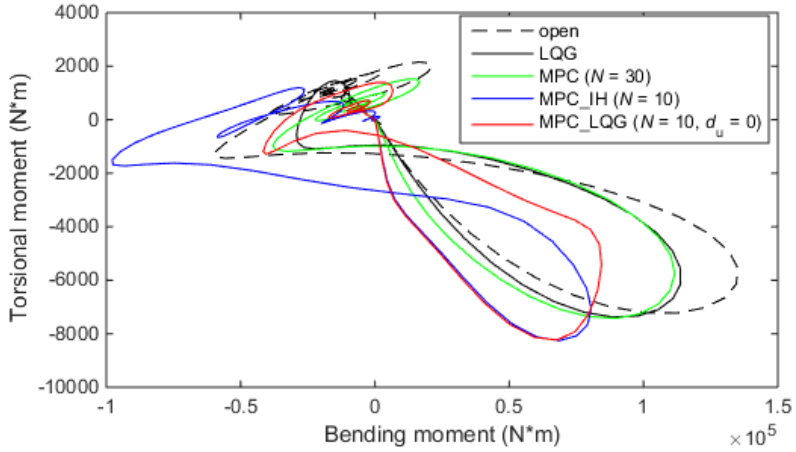

Fig. 9. Bending-torsion diagram of wing root for each controller

During the simulation process, the maximal computation time of the QP problem is found to be 11.4 ms on a laptop with 2.7 GHz processor. Considering that the sampling time is 5 ms, choosing d_u = 3 is enough to guarantee the applicability of the MPC_LQG method. Note that the calculation time can be reduced by using better computer hardware or more efficient QP solvers [40], but these will not be

considered here since the focus is to prove the effectiveness of the proposed MPC algorithm. Besides, supposing a large computation time also leaves space for other factors of control delay. The simulation results are shown in Fig. 10. Apparently, the GLA performance in Fig. 8 is perfectly retained.

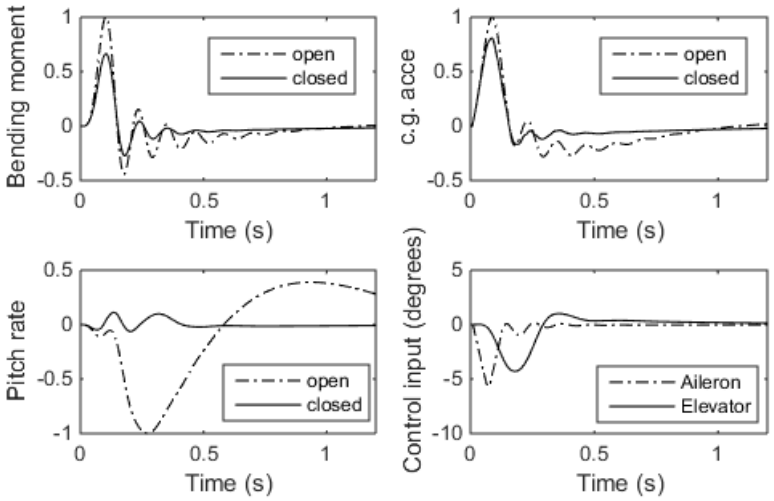

Fig. 10. Control performance of the MPC_LQG controller (N = 10, d_u = 3)

For easier comparison, the previous simulation results are summarized in Table 2, where the percentage reduction of the maximum values and the RMS values of different outputs are given. The wing root bending moment, the aircraft pitch rate, and the c.g. acceleration are denoted by M_{bend}, R_{pitch} and A_{cg}, respectively. As discussed before, the MPC_LQG method gives the best GLA performance. Afterwards, a control delay of 3 sampling periods is then added in the simulation and the results of different methods are shown in Table 3, noting that the method to deal with control delay is applied to the MPC_LQG method. Compared to Table 2, it is obvious that both the LQG method and the MPC_LQG method have subtle loss of control performance while the other two methods experience significant performance degradation. In a word, by using the method to deal with control delay in Section 3, the advantages of the MPC_LQG method is retained.

Table 2. GLA performance of different controllers without control delay

Methods	Percentage reduction of maximum values (%)			Percentage reduction of RMS values (%)		
	M_{bend}	A_{cg}	R_{pitch}	M_{bend}	A_{cg}	R_{pitch}
LQG	15.85	5.95	35.71	18.97	10.04	44.54
MPC (N = 30)	17.43	13.60	78.04	21.88	20.57	89.44
MPC_IH (N = 10)	27.61	25.30	55.65	10.79	27.06	74.66
MPC_LQG (N = 10, d_u = 0)	37.58	21.42	88.64	38.77	28.89	92.58

* Plant model: M = 0.4, H = 5 km. Internal model: M = 0.4, H = 5 km.

Table 3. GLA performance of different controllers with control delay of 3 sampling periods

Methods	Percentage reduction of maximum values (%)			Percentage reduction of RMS values (%)		
	M_{bend}	A_{cg}	R_{pitch}	M_{bend}	A_{cg}	R_{pitch}
LQG	13.81	3.94	33.02	19.38	9.66	43.98
MPC (N = 30)	8.50	6.01	64.81	12.05	14.15	71.85
MPC_IH (N = 10)	12.87	9.04	69.20	-14.97	5.50	72.49
MPC_LQG (N = 10, d_u = 3)	33.66	19.07	88.73	35.30	25.78	92.11

* Plant model: M = 0.4, H = 5 km. Internal model: M = 0.4, H = 5 km.

Due to explicit consideration of input constraints in the MPC controller, the actuator is allowed to reach control saturation to maximize the control performance. This is verified by the simulation results shown in Fig. 11, where the MPC_LQG method is applied to the case L_g = 110 m. Through a series of

simulation, the MPC_LQG method is verified to be always effective for the gust cases in Fig. 3, but these results are not shown here owing to space limitation.

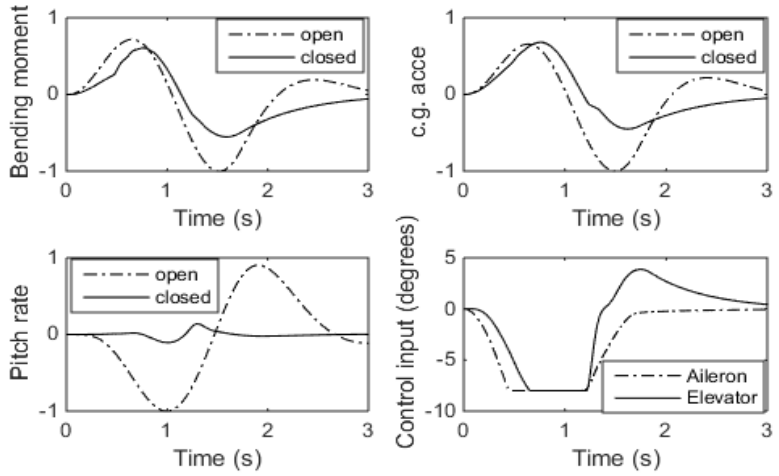

Fig. 11. Control performance of the MPC_LQG controller when L_g = 110 m (N = 10, d_u = 3)

In remark 3, the simple method to deal with constraints on $\boldsymbol{u}(k+i\,|\,k),\ i=N, N+1, \cdots, \infty$ in Eq. (37) is discussed, which is equivalent to relaxing the constraints on the control input in Eq. (37). Apart from the previous results, the reasonability of this method is further validated by comparing the performance of the MPC_LQG controller with different values of N, which is shown in Fig. 12. Since $N \geq d_u$ must be satisfied, the minimum value of N is 3 when d_u = 3. From Fig. 12, it is found that the MPC_LQG method has GLA effects even for the smallest N, and that the control performance is good enough when N = 6.

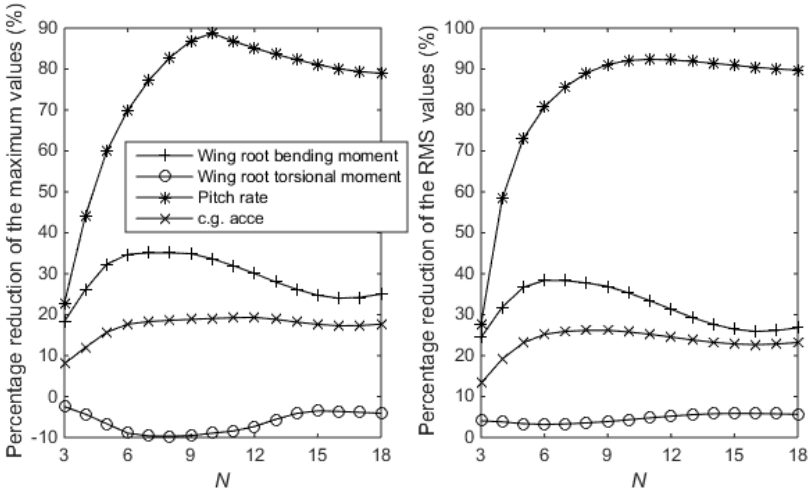

Fig. 12. Control performance of the MPC_LQG controller for different values of N (d_u = 3)

4.3 Comparison of control performance using only ailerons

To illustrate the importance of the elevators on gust response alleviation, only the ailerons are then used as the control surfaces and the control results for the worst gust case are depicted in Fig. 13. Through comparing Fig. 10 and Fig. 13, the following phenomena are observed. Firstly, the reduction of wing root bending moment is similar for the two cases. Secondly, the control performance of c.g. acceleration is slightly reduced for the latter case. Thirdly, the control performance the pitch rate is lost for the latter case. These are due to the fact that, for the current airplane configuration, the ailerons are vital for the control of elastic modes while the elevators are vital for the control of rigid modes. Furthermore, it is also obvious that better control of rigid modes contributes to faster convergence rates of all the quantities considered.

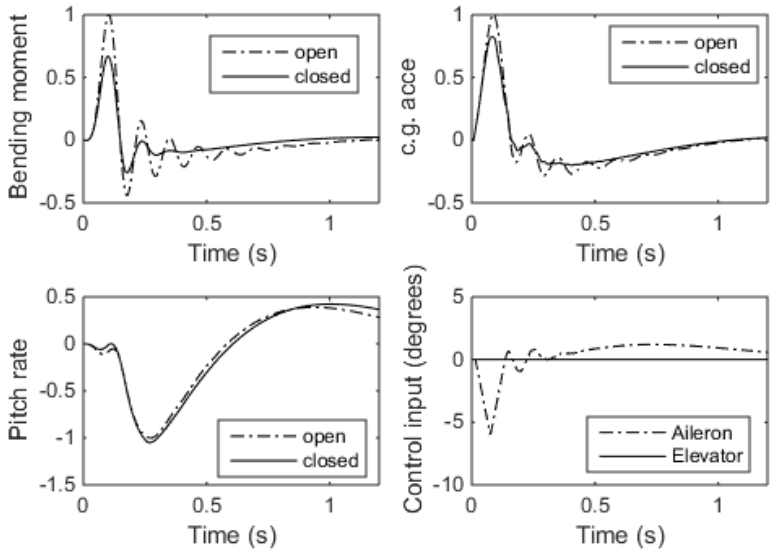

Fig. 13. Control performance of the MPC_LQG controller using only aileron (N = 10, d_u = 3)

4.4 Robust performance verification

The above results are all based on the assumption that there is no difference between the plant model and the internal model. Actually, although sometimes very small, this difference always exists. Therefore, robust stability and performance of the controller is required. This paper verifies the robust property of the MPC_LQG controller through altering certain parameters of the internal model, including the flight parameter and the structural parameter.

After changing the Mach number of the internal model from 0.4 to 0.5, the GLA performance of different controllers are given in Table 4 (with no control delay considered) and Table 5 (with a control delay of 3 sampling periods considered). Similarly, Tables 6~7 shows the results as the Mach number of the internal model is changed from 0.4 to 0.3. Through comparing these results with those in Tables 2~3, the following conclusion can be made: large difference between the plant model and the internal model leads to performance variations of different controllers, which is closely related to the accuracy of the predicted equation, while the MPC_LQG controller always has the best GLA performance and its performance variations are small.

Table 4. GLA performance of different controllers without control delay

Methods	Percentage reduction of maximum values (%)			Percentage reduction of RMS values (%)		
	M_{bend}	A_{cg}	R_{pitch}	M_{bend}	A_{cg}	R_{pitch}
LQG	12.84	6.71	52.41	15.39	10.43	52.91
MPC (N = 30)	6.94	10.01	62.54	11.33	16.95	74.13
MPC_IH (N = 10)	28.57	24.81	56.83	11.18	26.73	71.76
MPC_LQG (N = 10, d_u = 0)	30.76	21.48	74.09	31.24	27.04	74.08

* Plant model: M = 0.4, H = 5 km. Internal model: M = 0.5, H = 5 km.

Table 5. GLA performance of different controllers with control delay of 3 sampling periods

Methods	Percentage reduction of maximum values (%)			Percentage reduction of RMS values (%)		
	M_{bend}	A_{cg}	R_{pitch}	M_{bend}	A_{cg}	R_{pitch}
LQG	13.17	4.35	51.70	17.53	10.27	53.06
MPC (N = 30)	3.79	4.62	59.92	7.78	12.77	63.12
MPC_IH (N = 10)	12.73	8.93	67.71	-12.08	6.93	74.08
MPC_LQG (N = 10, d_u = 3)	27.77	19.27	74.94	28.32	24.17	73.13

* Plant model: M = 0.4, H = 5 km. Internal model: M = 0.5, H = 5 km.

Then, Table 8 gives performance of the MPC_LQG controller for the worst gust when there are changes in the structural property of the internal model. Specifically, the first elastic modal frequency

of the plant model is changed to test the robust performance of the MPC_LQG controller. The negative values in the first column represent decrease of the modal frequency. It is obvious that variations of the GLA performance are rather small. Although not shown here, this conclusion holds for other elastic modal frequencies. Furthermore, the closed-loop stability is still guaranteed when the frequency decreases by 40 percent, while a 30 percent decrease will lead to closed-loop instability for the traditional MPC controller with $N = 30$.

In a word, the results in Tables 4~8 validate the robust performance of the MPC_LQG controller.

Table 6. GLA performance of different controllers without control delay

Methods	Percentage reduction of maximum values (%)			Percentage reduction of RMS values (%)		
	M_{bend}	A_{cg}	R_{pitch}	M_{bend}	A_{cg}	R_{pitch}
LQG	13.30	5.02	25.92	18.30	9.63	40.40
MPC ($N = 30$)	30.68	18.71	67.96	33.92	25.37	74.39
MPC_IH ($N = 10$)	27.37	25.60	53.48	8.17	26.05	74.02
MPC_LQG ($N = 10$, $d_u = 0$)	41.01	21.73	74.29	41.95	30.44	76.17

* Plant model: M = 0.4, H = 5 km. Internal model: M = 0.3, H = 5 km.

Table 7. GLA performance of different controllers with control delay of 3 sampling periods

Methods	Percentage reduction of maximum values (%)			Percentage reduction of RMS values (%)		
	M_{bend}	A_{cg}	R_{pitch}	M_{bend}	A_{cg}	R_{pitch}
LQG	10.28	3.23	23.72	8.15	7.78	39.01
MPC ($N = 30$)	12.21	7.17	48.82	14.77	14.73	56.33
MPC_IH ($N = 10$)	12.78	9.43	68.40	-17.37	4.27	65.59
MPC_LQG ($N = 10$, $d_u = 3$)	35.96	19.04	72.66	38.68	27.16	74.81

* Plant model: M = 0.4, H = 5 km. Internal model: M = 0.3, H = 5 km.

Table 8. GLA performance of the MPC_LQG controller with variation of the first elastic modal frequency ($N = 10$, $d_u = 3$)

Percent increase	Percentage reduction of maximum values (%)			Percentage reduction of RMS values (%)		
	M_{bend}	R_{pitch}	A_{cg}	M_{bend}	R_{pitch}	A_{cg}
0	33.66	19.07	88.73	35.30	25.78	92.11
10	32.44	19.03	89.15	33.20	24.99	91.92
20	31.54	18.98	89.34	31.40	24.40	91.78
-10	34.91	19.17	88.12	37.30	26.68	92.32
-20	35.55	19.28	87.45	38.66	27.45	92.38

* Plant model: M = 0.4, H = 5 km. Internal model: M = 0.4, H = 5 km.

5. Conclusions

This paper proposes a LQG based MPC method for the purpose of active gust load alleviation, utilizing look-ahead information of the turbulence via LIDAR systems or on board alpha probe. To guarantee the nominal stability of the traditional MPC technique, the prediction horizon is first extended to infinity. Then, for the QP problem considered at each sampling time, an LQG controller is further assumed to be applied after given numbers of optimized control moves. This corresponds to extending the control horizon to infinity. The novelty of this framework lies in the realization of both infinite prediction horizon and infinite control horizon in the MPC algorithm, which contribute to improved robust stability and improved robust performance. Effectiveness and advantages of the proposed MPC framework are proved by a series of numerical results on a general transport aircraft model. In addition, a new technique to deal with control delay is also proposed and validated.

Conflict of interest statement

None declared.

Acknowledgement

This work is supported by the Industry-University Research Project of China Aviation Industry Corporation (Grant No. Cxy2010xG18) and the scholarship of China Scholarship Council (Grant No. CSC201606290144). The authors are grateful for the financial support.

Reference

[1] Gangsaas, D., Ly, U. and Norman D. C. (1981). "Practical gust load alleviation and flutter suppression control laws based on a LQG methodology." AlAA 19th Aerospace Sciences Meeting, American Inst. Aeronautics and Astronautics Inc., New York, 1-10.

[2] Vartio, E., Shimko, A., Tilmann, C. P. and Flick, P. M. (2005). "Structural modal control and gust load alleviation for a SensorCraft concept." 46th AIAA/ASME/ASCE/AHS/ASC Structures, Structural Dynamics & Materials Conference, American Inst. Aeronautics and Astronautics Inc., New York, 1-9.

[3] Aouf, N., Boulet, B. and Botez, R. (2000). "H2 and H_∞-optimal gust load alleviation for a flexible aircraft." Proceedings of the American Control Conference, IEEE, Piscataway, NJ, 1872-1876.

[4] Cook, R. G., Palacios, R. and Goulart, P. (2013). "Robust gust alleviation and stabilization of very flexible aircraft." AIAA Journal, 51(2), 330–340.

[5] Smain, D. and Brahim, B. (2010). "μ-synthesis controller design GLA for the longitudinal flexible aircraft." 2010 International Conference on Computer Applications and Industrial Electronics, IEEE, Piscataway, NJ, 558-563.

[6] Liu, X. and Sun, Q. (2016). "Gust load alleviation with robust control for a flexible wing." Shock and Vibration, Vol 2016, 1-10.

[7] Hahn, K. U. and Koenig, R. (1992). "ATTAS flight test and simulation results of the advanced gust management system LARS." Guidance, Navigation and Control Conference DLR.

[8] Dornheim, M. A. (1988). "Manufacturers see evolutionary change to handle turbulence." Aviation Week and Space Technology, 149(4), 76–79.

[9] Hecker, S. and Hahn, K. U. (2007). "Advanced gust load alleviation system for large flexible aircraft". 1st CEAS European Air and Space Conference, Berlin, Germany.

[10] Alam, M., Hromcik, M. and Hanis, T. (2015). "Active gust load alleviation system for flexible aircraft: Mixed feedforward/feedback approach." Aerospace Science and Technology, 41, 122-133.

[11] Zeng, J., Moulin, B., de Callafon, R. and Brenner, M. J. (2010). "Adaptive Feedforward Control for Gust Load Alleviation." Journal of Guidance, Control and Dynamics, 33(3), 862-872.

[12] Wildschek, A., Bartosiewicz, Z. and Mozyrska, D. (2014). "A multi-input multi-output adaptive feed-forward controller for vibration alleviation on a large blended wing body airliner." Journal of sound and vibration, 333(7), 3859-3880.

[13] Zhao, Y., Yue, C. and Hu, H. (2016). "Gust Load Alleviation on a Large Transport Airplane." Journal of Aircraft, 53(6), 1932-1946.

[14] Fonte, F., Ricci, S. and Mantegazza, P. (2015). "Gust load alleviation for a regional aircraft through a static output feedback." Journal of Aircraft, 52(5), 1559-1574.

[15] Lew, J., and Juang, J. (2012). "Robust generalized predictive control with uncertainty quantification." Journal of Guidance Control and Dynamics, 35(3), 930–937.

[16] Dai, Y., Yang, C., and Wang, C. (2017). "Strategy for robust gust response alleviation of an aircraft model." Control Engineering Practice, 60, 211-217.

[17] Heinze, S., and Karpel, M. (2006). "Analysis and wind tunnel testing of a piezoelectric tab for aeroelastic control applications." Journal of aircraft, 43(6), 1799-1804.

[18] Bi, Y., Xie, C., An, C., and Yang, C. (2017). "Gust load alleviation wind tunnel tests of a large-aspect-ratio flexible wing with piezoelectric control." Chinese Journal of Aeronautics, 30(1), 292-309.

[19] Cooper, J. E., Chekkal, I., Cheung, R. C. M., Wales, C., Allen, N. J., Lawson, S., ... and Carossa, G. M. (2015). "Design of a morphing wingtip." Journal of Aircraft, 52(5), 1394-1403.

[20] Castrichini, A., Cooper, J. E., Wilson, T., Carrella, A., and Lemmens, Y. (2016). "Nonlinear negative stiffness wingtip spring device for gust loads alleviation." Journal of Aircraft, Vol. 54, Special Section on Cranked Arrow Wing Aerodynamics Project International II/F-16XL, 627-641.

[21] Haghighat, S., Liu, H. H. T. and Martins, J. R. R. A. (2012). "A Model Predictive Gust Load Alleviation Controller for a Highly Flexible Aircraft". Journal of Guidance Control & Dynamics, 35(6), 1751-1766.

[22] Wang, Y., Wynn, A. and Palacios, R. (2016). "Model-Predictive Control of Flexible Aircraft Dynamics using Nonlinear Reduced-Order Models". AIAA/ASCE/AHS/ASC Structures, Structural Dynamics, and Materials Conference.

[23] Giesseler, H. G., Kopf, M., Varutti, P., Faulwasser, T., and Findeisen, R. (2012). "Model Predictive Control for Gust Load Alleviation". Ifac Nonlinear Model Predictive Control Conference, Noordwijkerhout, Nl, Vol.45, 27-32.

[24] Kopf, M., Giesseler, H. G., Varutti, P., and Faulwasser, T. (2015). "On the effect of enforcing stability in model predictive control for gust load alleviation". American Control Conference, 2329-2334.

[25] Slegers, N., Kyle, J. and Costello, M. (2006). "Nonlinear Model Predictive Control Technique for Unmanned Air Vehicles." Journal of Guidance Control & Dynamics 29(5), 1179-1188.

[26] Richards, A. and How, J. P. (2006). “Robust variable horizon model predictive control for vehicle maneuvering”. International Journal of Robust & Nonlinear Control, 16(7), 333–351.
[27] Gibbens, P. W. and Medagoda, E. D. B. (2011). "Efficient Model Predictive Control Algorithm for Aircraft", Journal of Guidance, Control, and Dynamics, 34(6), 1909-1915.
[28] Ricker, N. L. (1990). “Model predictive control with state estimation”. Ind.eng.chem.res, 29(3), 374-382.
[29] Liu, X. and Sun, Q. (2017). “Improved LQG method for Active Gust Load Alleviation”. Journal of aerospace engineering, 30(4). 04017006.
[30] Moulin, B. and Karpel, M. (2007). “Gust Loads Alleviation Using Special Control Surfaces”. Journal of Aircraft, 44(1), 17-25.
[31] Azoulay, D. and Karpel, M. (2006). “Characterization of methods for computation of aeroservoelastic response to gust excitation.” American Institute of Aeronautics and Astronautics Inc., Reston, VA, 1–15.
[32] Kwon, W. and Han, S. (2005). “Receding Horizon Control: Model Predictive Control for State Models”, Springer, New York.
[33] Abate, A. and Ghaoui, L. E. (2004). “Robust Model Predictive Control Through Adjustable Variables: An Application to Path Planning,” 43rd IEEE Conference on Decision and Control, Berkeley, CA, Dec.
[34] Boyd, S. and Vandenberghe, L. (2004). “Convex Optimization”, Cambridge Univ. Press, Cambridge, England, U.K.
[35] Mayne, D. Q., Rawlings, J. B., Rao, C. V., and Scokaert, P. O. M. (2000). “Constrained Model Predictive Control: Stability and Optimality,” Automatica, 36(6), 789–814.
[36] Batina, I. (2004). “Model Predictive Control for Stochastic Systems by Randomized Algorithms,” Ph.D. Thesis, Technische Universiteit, Eindhoven, Netherlands.
[37] Huang, R., Hu, H., Zhao, Y. (2012). “Designing active flutter suppression for high-dimensional aeroelastic systems involving a control delay”. Journal of Fluids and Structures, 34(4), 33-50.
[38] ZAERO. (2008). “Application’s manual vol. 2: Discrete gust loads sample cases.” ZONA Technology, Inc., Scottsdale, 121–198.
[39] “Certification Specifications and Acceptable Means of Compliance for Large Aeroplanes CS-25,”Amendment 19, Annex to ED Decision 2017/015/R, European Aviation Safety Agency, May 2017.
[40] Wang, Y. and Boyd, S. (2010). “Fast model predictive control using online optimization”. IEEE Transactions on Control Systems Technology, 18(2), 267-278.